Journal of Catalysis 262 (2009) 257–265

Contents lists available at ScienceDirect

Journal of Catalysis

www.elsevier.com/locate/jcat

Synthesis and characterization of mesoporous mordenite

Xianfeng Li [a,b], Roel Prins [a], Jeroen Anton van Bokhoven [a,*]

[a] Institute for Chemical and Bioengineering, Swiss Federal Institute of Technology (ETH), 8093 Zurich, Switzerland
[b] Faculty of Chemical Science and Engineering, China University of Petroleum, 102249 Beijing, PR China

ARTICLE INFO

Article history:
Received 31 October 2008
Revised 19 December 2008
Accepted 4 January 2009
Available online 22 January 2009

Keywords:
Mesopore
Mordenite
Leaching
Alkylation
Isomerization
Diffusivity

ABSTRACT

Three methods were investigated to synthesize mesoporous mordenite. XRD, N_2 physisorption, SEM, and TEM showed that the mordenite obtained by acid leaching followed by base leaching of a conventional mordenite is a crystalline mesoporous material with MOR framework. The higher diffusivity of toluene indicated that mesopores benefited molecule transport through the zeolite crystal. Measurement of the number of Brønsted acid sites by *n*-propylamine TPD and ^{27}Al NMR showed that the mesoporous mordenite had less extra-framework aluminum and a large number of Brønsted acid sites, while the isomerization of 2-methyl-2-pentene indicated that the mesoporous mordenite possessed a higher reactivity than conventional mordenite. The mesoporous mordenite had a much higher catalytic activity than conventional mordenite in the alkylation of benzene with benzyl alcohol. At 353 K and under atmospheric pressure, the conversion of benzyl alcohol over hierarchical mesoporous mordenite was 100% in 3 h, whereas the conversion over conventional mordenite was less than 2%. Synthesis of mesoporous mordenite with amphiphilic organosilane and carbon as secondary template did not give real mesoporous mordenite.

1. Introduction

Mordenite is a zeolite with two-dimensional pores, as the structure determined by Meier in 1961 showed [1]. The pore system of mordenite consists of main channels of 6.5 × 7.0 Å, which are connected by tortuous pores of 2.6 × 5.7 Å that form the so-called side pockets. Since the latter are too small for most molecules to enter, mordenite is generally regarded as a mono-dimensional zeolite. Mordenite is widely used in catalysis and in separation and purification because of its uniform, small pore size, high internal surface area, flexible framework, and controlled chemistry. The major drawback of mordenite and zeolites in general is the limited size of the channels and cavities and the lack of interconnectivity. This imposes diffusional limitations on reactions, limiting their activity, selectivity, and stability. It has been repeatedly demonstrated that mass transfer limitations play an important role in industrial applications using zeolites [2–5].

In recent years, various strategies have been developed to synthesize mesoporous zeolites to enhance their pore accessibility. The generation of mesopores in zeolite crystals results in shorter intracrystalline diffusion path lengths and higher external surface areas. Mesopores have been obtained by synthesis of zeolite nanoparticles [6–8], steaming [9–11], acid leaching [12–14], base leaching [15–17], and by using soft [18] and hard templates [19–21] during synthesis.

In the present work, we compare three methods to obtain mesoporous mordenite: acid leaching followed by base leaching, soft templating using [3-(trimethoxysilyl)propyl][hexadecyldimethyl-ammonium] chloride (TPHAC), and hard templating using carbon black. The performance of mesoporous mordenite was compared in the liquid phase alkylation of benzene with benzyl alcohol [22–24] and in the isomerization of 2-methyl-2-pentene [25].

2. Experimental

2.1. Catalyst preparation

2.1.1. Zeolite synthesis

Mordenite with a Si/Al ratio of 15 was hydrothermally synthesized according to Ref. [26]. The composition of the gel was $6Na_2O{:}Al_2O_3{:}30SiO_2{:}780H_2O$. $NaAlO_2$ (Strem Chemicals, 92%) as the aluminum source was mixed with an aqueous solution of NaOH (Aldrich, 99.998%). Then fumed silica (Aldrich, 99.8%) was added to the mixture and the mixture was homogenized by stirring. Finally, the gel was transferred to a Teflon-lined autoclave and crystallization was carried out at 453 K under autogenous pressure without agitation for 24 h. The product was recovered by filtration, washed thoroughly with deionized water and dried at 393 K overnight, then calcined in air at 823 K for 2 h. The mordenite was then ion-exchanged three times with a 1 M NH_4NO_3 (Fluka, 99%)

* Corresponding author.
E-mail address: jeroen.vanbokhoven@chem.ethz.ch (J.A. van Bokhoven).

0021-9517/$ – see front matter
doi:10.1016/j.jcat.2009.01.001

solution under stirring for 1 h at 353 K and calcined in air at 823 K for 4 h to convert it into the H^+ form. The resulting sample was named HMOR-parent.

2.1.2. Leaching

HMOR-parent was treated with 0.2 M NaOH (Aldrich, 99.998%) at 338 K for 30 min and subsequently washed with deionized water and dried at 393 K for 10 h, then calcined at 823 K for 2 h. Thereafter, the mordenite was ion-exchanged three times with a 1 M NH_4NO_3 (Fluka, 99%) solution under stirring for 1 h at 353 K and then calcined in air at 823 K for 4 h to get HMOR-parent-A.

HMOR-parent was treated with 2 M HNO_3 (Merck, 65%) at 373 K for 4 h under reflux and subsequently washed with deionized water and dried at 393 K for 10 h, then calcined at 823 K for 2 h to get HMOR-acid. 1.8 g HMOR-acid was treated in 0.2 M NaOH as described above for the transformation of HMOR-parent into HMOR-parent-A. The sample resulting from base leaching of HMOR-acid is called HMOR-A. By using different amounts of NaOH solution, the samples HMOR-A1 (0.2 M NaOH, 72 ml) and HMOR-A2 (0.2 M NaOH, 87 ml) were obtained.

2.1.3. Soft templating

TPHAC was prepared according to a reported procedure [27], and was added to a mixture containing NaOH (Aldrich, 99.998%), fumed silica (Aldrich, 99.8%), $NaAlO_2$ (Strem Chemicals, 92%), and distilled water. The composition of the resulting gel was $6Na_2O{:}Al_2O_3{:}30SiO_2{:}1.58TPHAC{:}780H_2O$. The gel was transferred to a Teflon-lined autoclave and crystallization was carried out at 453 K under autogenous pressure with agitation for 48 h. The product was recovered by filtration, washed thoroughly with deionized water and dried at 393 K overnight, then calcined in air at 823 K for 6 h. Finally, the sample was ion-exchanged three times with a 1 M NH_4NO_3 (Fluka, 99%) solution under stirring for 1 h at 353 K and then calcined in air at 823 K for 4 h. The sample was named HMOR-TPHAC.

2.1.4. Hard templating

A mordenite sample was synthesized by hard templating according to Ref. [28]. About 10 g of BP-2000 carbon (Carbot Corporation) was dried in an oven at 393 K overnight. In a 160 ml flask, 0.854 g NaOH (Aldrich, 99.998%), 29.835 g of H_2O and 0.380 g of $NaAlO_2$ (Strem Chemicals, 92%) was added and heated briefly with stirring until a clear solution was obtained. After cooling to room temperature 15.1 g of ethanol was added with stirring to obtain a homogeneous solution. The carbon was impregnated with this solution to incipient wetness. After evaporation of the ethanol at room temperature in the open air for 12 h, the carbon particles were impregnated with 13.478 g of TEOS (Fluka, 99%). This mixture was left to hydrolyze overnight. The composition of the resulting synthesis gel was $6Na_2O{:}Al_2O_3{:}30SiO_2{:}780H_2O$. The gel was transferred to a Teflon-lined autoclave and crystallization was carried out at 453 K under autogenous pressure without agitation for 48 h. The product was recovered by filtration, washed thoroughly with deionized water, dried at 393 K overnight, and calcined in air at 823 K for 10 h. Finally the sample was ion-exchanged three times with a 1 M NH_4NO_3 (Fluka, 99%) solution under stirring for 1 h at 353 K and then calcined in air at 823 K for 4 h. The resulting sample was named HMOR-carbon.

2.2. Characterization

Powder X-ray diffraction (XRD) was employed to identify the samples. X-ray diffractograms were recorded on a Siemens D5000 powder diffraction system using Cu$K\alpha$ radiation (45 kV and 35 mA) and Cu as the reference. Nitrogen sorption isotherms were measured at 77 K on a Micromeritics Tristar instrument; the sample was outgassed at 523 K for 2 h under 10^{-3} Pa before the measurement. The bulk Si/Al ratios of the zeolites were determined by ICP-OES on a Perkin-Elmer Optima 4300DV instrument.

Scanning electron microscopy (SEM) was performed on selected representative samples to determine the crystallite size and morphology. The SEM images were obtained on a Gemini 1530 (Zeiss) instrument at low voltage (in most cases 1 keV). Transmission electron microscopy (TEM) measurements were performed on selected representative samples to determine the mesopore structure. For the TEM investigation, the material was deposited onto a holey carbon foil supported on a copper grid. TEM investigations were performed with a CM30ST microscope (Philips; LaB6 cathode, operated at 300 kV, point resolution ~2 Å).

^{27}Al MAS NMR experiments were performed at room temperature on a Bruker Advance 500 spectrometer at a resonance frequency of 130.34 MHz using a 4 mm probe. In the experiments, a single pulse length of $\pi/4$ and a relaxation delay of 0.5 s, and a spinning rate of ca. 8 kHz were used. The ^{27}Al chemical shift was referenced to $(NH_4)Al(SO_4)_2{\cdot}12H_2O$.

For the preparation of a sample for the temperature-programmed reaction of *n*-propylamine, approximately 20–40 mg sample were activated at $P < 10^{-4}$ Pa overnight by heating to 723 K with a ramp of 2 K/min. The sample was then exposed to *n*-propylamine at 473 K for 2 h and cooled to room temperature. The sample was evacuated for about 2 h to remove physically adsorbed *n*-propylamine. The decomposition experiment was performed with a heating rate of 10 K/min and a flow of 20 ml/min helium in a Mettler Toledo TGA/SDTA851e thermogravimetric analysis (TGA) instrument. The amount of decomposed *n*-propylamine was obtained from the mass changes in the TGA curves between 573 and 873 K.

IR spectra were recorded in transmission mode on a Biorad Excalibur FTS 3000 IR spectrometer equipped with a MCT detector. Approximately 3 mg of each pre-calcined sample was pressed into a self-supporting pellet without KBr dilution. The samples were activated in a stream of helium at 673 K to remove moisture. After activation at 673 K the samples were measured at 373 K with a flow of 6 ml/min from 4000 to 1000 cm^{-1}. To correct for the varying sample thickness of the different wafers, the spectra were normalized by the integral intensity of the overtones of the lattice vibrational bands at 1972 and 1865 cm^{-1}.

2.3. Catalytic tests

2.3.1. Isomerization

The isomerization of 2-methyl-2-pentene (2M2P) was studied by passing the vapor of the alkene over 0.1 g catalyst contained in a quartz tube reactor whose inner diameter was 4 mm. Catalysts were pretreated in flowing helium for about 1 h at 723 K before use. The reaction was initially conducted at 473 K for 1 h, while flowing 15 ml/min of a mixture of 7% 2M2P in helium at atmospheric pressure over the catalyst. Then the feed was stopped and the catalyst allowed to cool to 423 K while flushing with helium. At this temperature, the 2M2P in helium feed was reintroduced into the reactor. After a reaction time of 10 min, the conversion and selectivity were determined. Products were analyzed online on an Agilent 6890 GC with an FID detector using a 50 m HP5 packed column.

2.3.2. Alkylation

The liquid phase benzylation of benzene with benzyl alcohol was carried out in a three-necked round-bottom flask equipped with a reflux condenser and heated in a temperature controlled oil bath under atmospheric pressure. In a typical run, 34 ml of benzene was added to 0.15 g catalyst, which had been activated

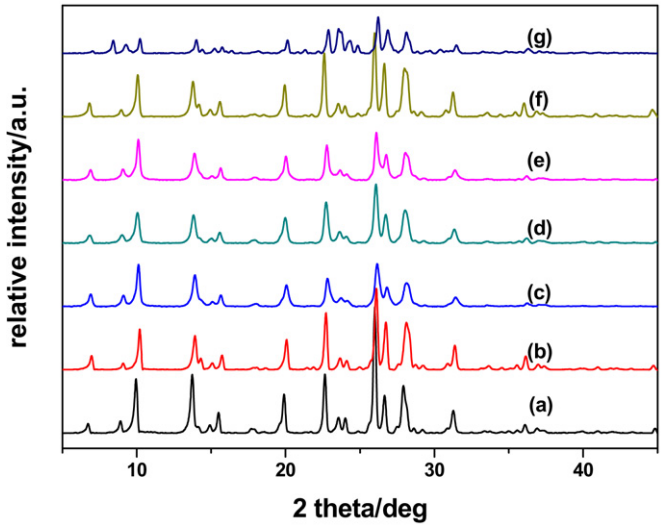

Fig. 1. XRD patterns of (a) HMOR-parent, (b) HMOR-acid, (c) HMOR-A1, (d) HMOR-A2, (e) HMOR-parent-A, (f) HMOR-TPHAC, (g) HMOR-carbon.

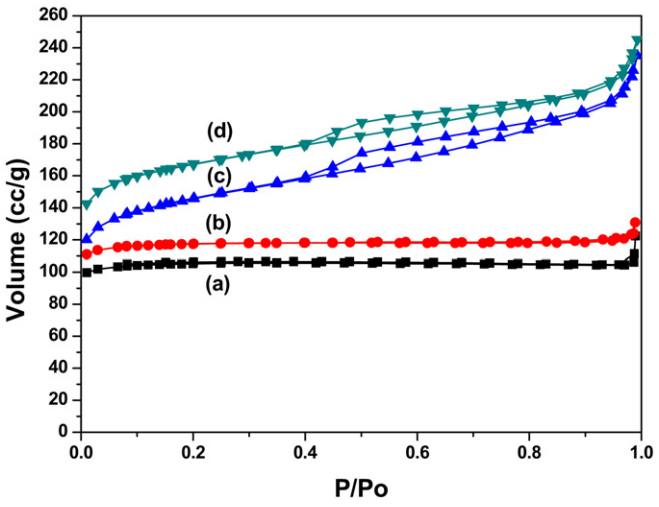

Fig. 2. N_2 adsorption and desorption isotherms of (a) HMOR-parent, (b) HMOR-acid, (c) HMOR-A1, (d) HMOR-A2 (d was offset in the way of *Y* axis).

at 773 K in air for 5 h. The reaction mixture was maintained for 30 min at the required reaction temperature and then 0.5 ml of benzyl alcohol was added. This moment of addition was taken as the initial reaction time. Liquid samples were withdrawn at regular intervals and analyzed by gas chromatography on an Agilent 6890 GC with an FID detector using a 50 m packed HP5 column. The products were identified by GC-MS analysis. The conversion was calculated based on the benzylating reagent, i.e. benzyl alcohol.

2.4. Diffusivity measurements

Thermo-gravimetric measurements were carried out in a Mettler Toledo TGA/SDTA851e instrument by using a modified thermo-gravimetric analysis system with on-line monitoring of mass changes. For an analysis, the mordenite powder was pressed into pellets under 5 ton pressure into pellets, which were crushed to particles of 60 mesh, and about 10 mg of the particle sample was loaded into the instrument. The particle sample was pretreated at 723 K in helium for 1 h and subsequently allowed to cool to 373 K. After stabilization of the particle sample weight, the zeolite was exposed to known amounts of toluene, which were transported by helium gas through a precalibrated mass-flow controller.

3. Results and discussion

3.1. Catalyst characterization

The XRD patterns of the mordenite zeolite samples display sharp reflection lines between 5° to 45° at the characteristic 2-theta positions of HMOR and show that highly crystalline mordenite has been formed in the HMOR-parent and HMOR-TPHAC samples (Fig. 1). The XRD patterns also demonstrate long-range crystal ordering in the HMOR-acid, HMOR-A1, HMOR-A2, and HMOR-parent-A samples. The intensity of their characteristic reflections was lower than of HMOR-parent, meaning that some crystallinity was lost during leaching. Ogura et al. [29] observed that silicon species were dissolved from relatively weaker parts of the ZSM-5 zeolite, such as growing faces, resulting in a better crystallinity of the remaining zeolite. Similarly, in our work, we observed that the intensity of the diffraction peak at 25.8° of HMOR-A2, for which more alkali solution was used for leaching than for HMOR-A1, was higher than that of HMOR-A1. At the same time, compared with HMOR-parent, the width of the peak at 25.8° of the HMOR-acid, HMOR-A1, HMOR-A2, and HMOR-parent-A samples

Table 1
Textural properties of the different mordenite samples.

Samples	S_{BET}[a] ($m^2\,g^{-1}$)	S_{ext}[b] ($m^2\,g^{-1}$)	V_{micro}[b] ($ml\,g^{-1}$)	V_{meso} ($ml\,g^{-1}$)
HMOR-parent	384	23	0.153	0.003
HMOR-parent-A	471	97	0.158	0.085
HMOR-acid	455	36	0.178	0.013
HMOR-A1	524	174	0.149	0.166
HMOR-A2	530	167	0.155	0.142
HMOR-TPHAC	378	166	0.090	0.257
HMOR-carbon	317	38	0.118	0.034

[a] BET method.
[b] *t*-Plot method.

was larger, which means that the grain sizes of these samples were smaller, because aluminum and silicon was extracted during leaching, and many cracks and faults were formed on the outer surface of zeolite grains, which leads to partial collapse of large particles into small particles. The XRD measurements also showed that the crystallinity of the HMOR-carbon sample was lower than that of the other samples and extra lines showed that the sample is not phase pure.

The adsorption/desorption branches in N_2 physisorption of the HMOR-parent and HMOR-acid samples were similar (Fig. 2); both belong to a Langmuir-type isotherm. After acid leaching, the micropore volume increased from 0.153 to 0.178 $ml\,g^{-1}$ and the surface area from 384 to 455 $m^2\,g^{-1}$ (Table 1). The increase in micropore volume after the acid treatment may be induced by an appreciable change in its size distribution of micropores [12]. The N_2 adsorption/desorption branches of the HMOR-acid sample did not show hysteresis, indicating that acid leaching did not create mesopores. The hysteresis loop in the N_2 adsorption isotherms of the alkali-treated mordenite appeared at higher relative pressures, indicating the absence of a major external surface area contribution. The isotherms of the HMOR-A1 and HMOR-A2 samples showed a continuously increasing slope and a hysteresis loop, which indicates the presence of mesopores. These shapes can be classified as H2 ink-bottle pores [30]. The mesopores may have been formed by opening two large pores of 6.5 × 7.0 Å as a result of the elimination of aluminum and silicon. Going from HMOR-parent to HMOR-acid to HMOR-A1, the surface area increased from 384 to 455 to 524 $m^2\,g^{-1}$, the external area from 23 to 36 to 174 $m^2\,g^{-1}$, and the mesopore volume from 0.003 to 0.013 to 0.166 $ml\,g^{-1}$ after acid and base leaching, respectively (Table 1), while the micropore volume increased from 0.153 $ml\,g^{-1}$ for HMOR-parent to 0.178 $ml\,g^{-1}$

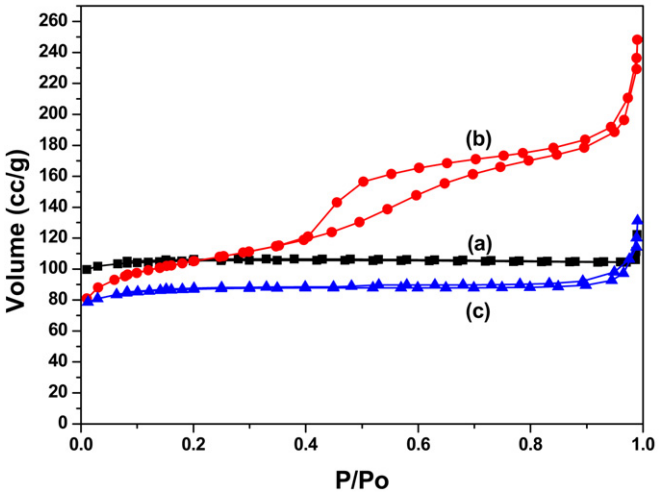

Fig. 3. N_2 adsorption and desorption isotherms of (a) HMOR-parent, (b) HMOR-TPHAC, (c) HMOR-carbon.

(HMOR-acid) and then decreased to 0.149 ml g^{-1} for HMOR-A1. These results suggest that maybe a transformation of micropores to mesopores occurred during the base leaching, because the extraction of silicon atoms from the mordenite framework produces mesopores through the collapse of pore walls of the micropores, which will lead to the micropore volume and area decrease obviously. However, some micropores were exposed because some amorphous silica blocked in the micropores was dissolved after the base leaching. So finally, the micropore volume and area only decreased a little.

Acid and base leaching appears to give the best combination of microporosity, high surface and external area, and high mesopore volume. In contrast, the textural data of HMOR-parent-A, that was obtained by direct base leaching, were not as good as those of HMOR-A1, probably because the Si/Al molar ratio of the starting material (HMOR-parent) was not in the optimal range. An optimal Si/Al range of 25–50 was found by Groen et al. for the extraction of silicon from zeolites, leading to well-controlled mesopore formation [31,32]. At lower Si/Al ratios the extraction of framework silicon is inhibited due to the protective role of aluminum, while at higher ratios excessive silicon extraction leads to the formation of very large pores. This is why we applied acid leaching preceding the base leaching. The acid leaching lowered the Al content of the mordenite and increased the Si/Al ratio of 15 of HMOR-parent to 25 of HMOR-acid and thus brought the ratio in the window in which base leaching is effective.

The shape of the nitrogen adsorption-desorption isotherm of HMOR-TPHAC showed a large hysteresis loop (Fig. 3), which is attributed to the presence of mesopores. A large mesopore volume was found in this sample (Table 1), it increased strongly from 0.003 to 0.257 ml g^{-1} compared with the HMOR-parent sample, but the BET surface area did not change and the micropore volume decreased, although the external area increased from 23 to 166 $m^2 g^{-1}$. The isotherm of HMOR-carbon showed a small hysteresis loop, and there was little mesopore formation (Table 1). The mesopore volume increased slightly from 0.003 to 0.034 ml g^{-1} compared with HMOR-parent, but the surface area decreased from 384 to 317 $m^2 g^{-1}$.

Fig. 4 shows the SEM images of the MOR crystals after different stages of leaching. They revealed that the parent sample consisted of aggregated plate-like sheets of ellipsoidal particles. After acid leaching, the crystal size and morphology of mordenite was not changed, but after alkali treatment cracking occurred and major surface roughness appeared. The TEM images of HMOR-parent and HMOR-acid were similar (Figs. 5a and 5b). No light spots were visible, indicating that no mesopores were formed during the acid leaching. A few bright spots appeared in the TEM images of HMOR-A1 and A2 (Figs. 5c and 5d), corresponding to holes in the crystals, which could be mesopores. Thus, the investigations revealed that a crystalline material with mesopores was obtained after acid and base leaching.

The SEM and TEM micrographs of HMOR-TPHAC (Fig. 6) indicated that this sample contained two phases, a crystalline and an amorphous phase. These images suggest that the large hysteresis loop in the N_2 isotherms comes from amorphous material, not from the crystalline zeolite material. Fig. 7 shows that there are also two phases in the HMOR-carbon sample, but more crystalline material was visible, explaining why the mesopore volume was lower. Some amorphous silica appeared on the surface of the crystals. On the other hand, the shape of the crystals differed from that of HMOR-parent, the pillars were longer and the shape was irregular.

Usually, mordenite crystals with a low Si/Al molar ratio are needle-shaped, mordenite crystals with a ratio between 10 and 15 form as plates, whereas crystals with a high ratio are flat and prismatic [33]. The shape of HMOR-parent agrees with this, but for HMOR-TPHAC and HMOR-carbon this is not the case, which may be explained by the presence of an impurity phase.

The acid treatment of the MOR zeolite extracted aluminum atoms from the zeolite framework, leading to a significant increase in its Si/Al molar ratio from 15 to 25, as determined by ICP (Table 2). Base leaching decreased the Si/Al molar ratio, because of extraction of silicon atoms from the framework. The Si/Al molar ratios of HMOR-TPHAC and HMOR-carbon were similar to that of HMOR-parent, because the same molar ratios were used in the synthesis.

^{27}Al MAS NMR spectroscopy provides information about the coordination of the aluminum species. The peak at 54 ppm corresponds to tetrahedrally coordinated Al^{VI} atoms in the framework and the −1 ppm signal belongs to Al^{VI} atoms extracted from the framework [34,35]. Acidic zeolites generally show the presence of a narrow octahedral peak in ^{27}Al MAS NMR [36–39]. Fig. 8 shows that all samples contain tetrahedral and octahedral aluminum, but that the concentration of the octahedrally coordinated aluminum (EFAl) is different. The parent mordenite contained more octahedrally coordinated aluminum (Table 2), but after acid and base leaching it decreased because the octahedrally coordinated aluminum was dissolved in the acid or base solution.

The number of Brønsted acid sites (bridged OH groups) is determined by the number of aluminum atoms in the framework of a zeolite [40–42]. The higher the framework Si/Al molar ratio, the lower is the number of Brønsted acid sites. The Si/Al molar ratios shown in Table 2 are bulk Si/Al molar ratios, which are different from the framework Si/Al molar ratios because there is EFAl in the samples. The real framework Si/Al molar ratios can be calculated from the ICP and NMR results. For instance, for the HMOR-parent, the bulk Si/Al molar ratio is 15 (ICP result), but only $100 - 23.2 = 76.8\%$ of the Al is in the framework (NMR result). Thus the framework Si/Al molar ratio is Si/(0.768Al) = 20. In the same way, the framework Si/Al molar ratio of HMOR-acid is 32, that of HMOR-A1 is 27, and that of HMOR-A2 is 25. As a consequence, the order of the number of Brønsted acid sites in the three samples is HMOR-parent > HMOR-A2 > HMOR-A1 > HMOR-acid. The TPD of *n*-propylamine showed the same order: HMOR-parent (1.24) > HMOR-A2 (1.22) > HMOR-A1 (1.20) > HMOR-acid (0.78) (Table 2). The order of the number of acid sites of the four samples is thus equal for the two methods of determination, by combined ICP-NMR and by TPD of *n*-propylamine. The framework Si/Al molar ratio of HMOR-parent, HMOR-A2, and HMOR-A1 is different (20, 25, and 27), but the number of Brønsted acid sites as determined by temperature-programmed reaction is almost equal

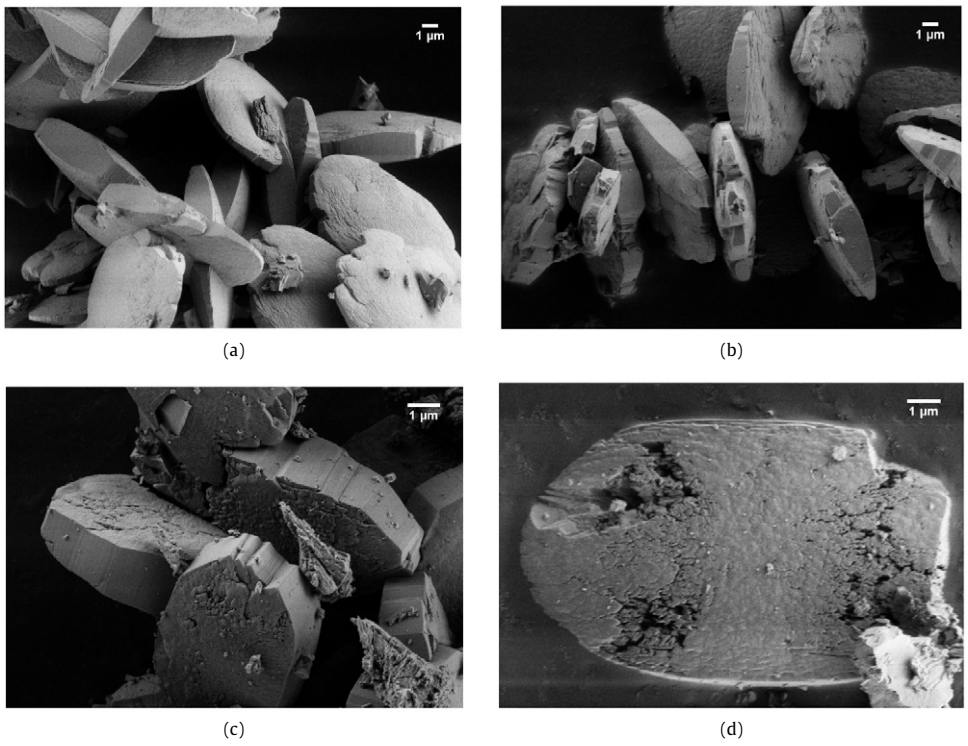

Fig. 4. SEM micrographs of (a) HMOR-parent, (b) HMOR-acid, (c) HMOR-A1, (d) HMOR-A2.

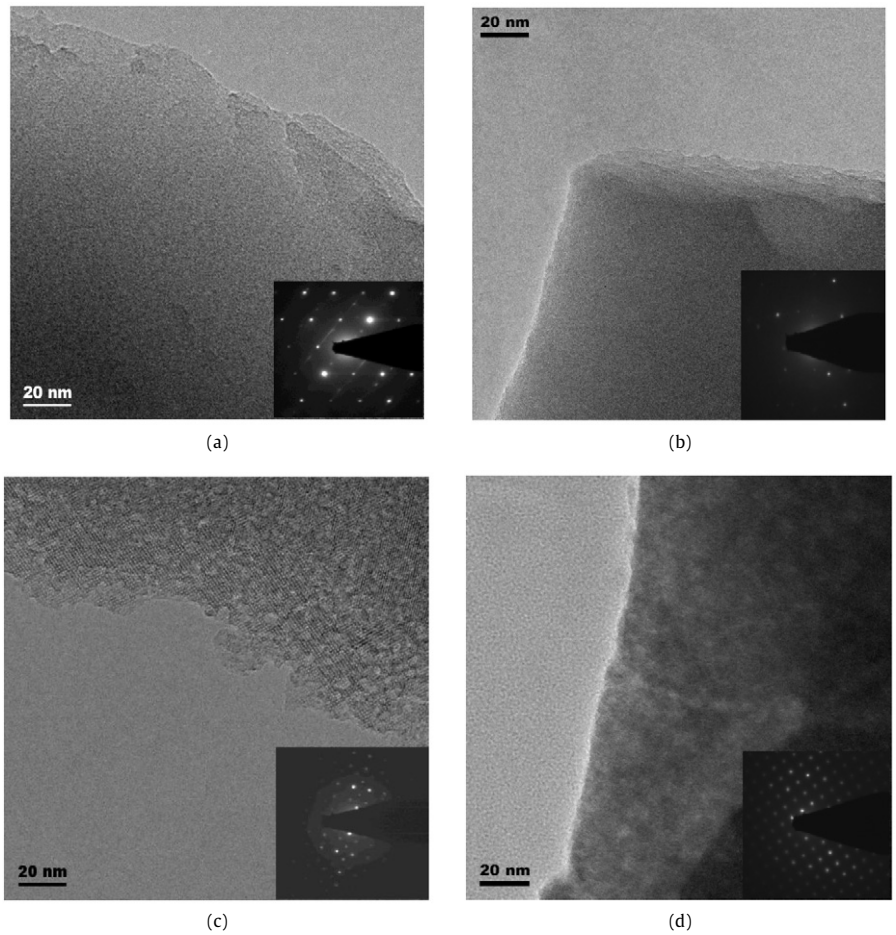

Fig. 5. TEM micrographs of (a) HMOR-parent, (b) HMOR-acid, (c) HMOR-A1, (d) HMOR-A2.

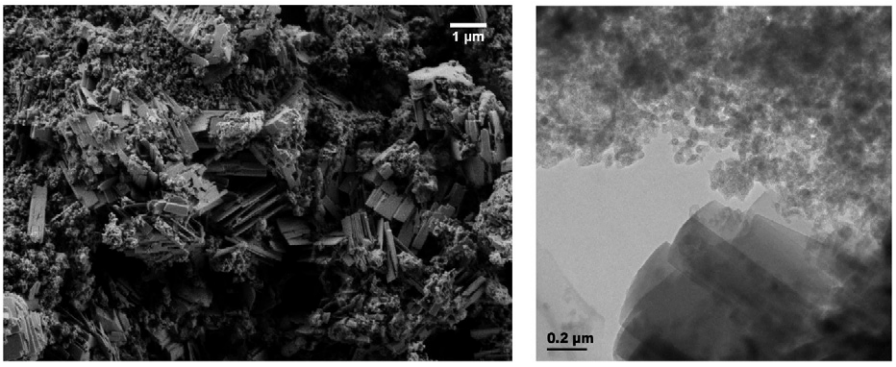

Fig. 6. SEM and TEM micrographs of HMOR-TPHAC.

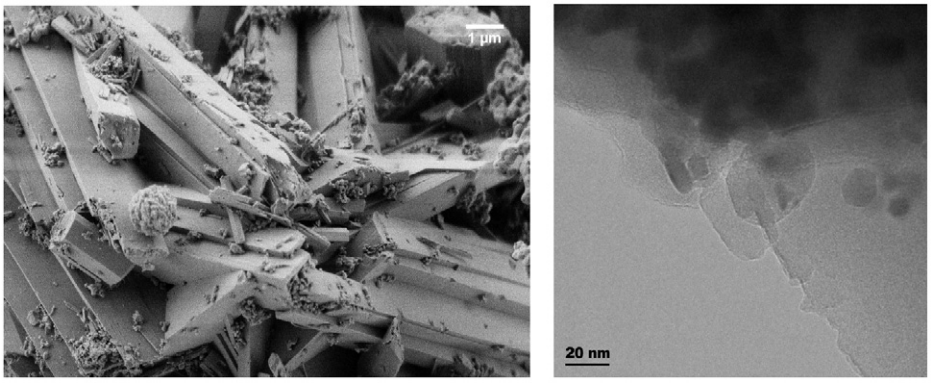

Fig. 7. SEM and TEM micrographs of HMOR-carbon.

Table 2
Acidity properties and chemical composition of the different mordenite samples.

Samples	Molar (Si/Al)[a]	EFAl (%)[b]	Brønsted acid sites (mmol/g)[c]
HMOR-parent	15	23.2	1.24
HMOR-acid	25	21.5	0.78
HMOR-A1	23	16.3	1.20
HMOR-A2	21	17.4	1.22
HMOR-TPHAC	14	22.4	n.d.[d]
HMOR-carbon	14	17.0	n.d.

[a] Determined by ICP analysis.
[b] Determined by ^{27}Al MAS NMR.
[c] Determined by the decomposition of *n*-propylamine.
[d] n.d., not determined.

(1.24, 1.22, and 1.20). This can be explained by the presence of extra framework Si. After base leaching, the silicon atoms extracted from the mordenite framework lead to a higher number of extra framework Si atoms in the HMOR-Al and HMOR-A2 samples than in the HMOR-parent and HMOR-acid samples, thus the real framework Si/Al molar ratio of HMOR-A1 is lower than 27 (HMOR-A2 is lower than 25). This explains the difference between the ICP-NMR and TPD results and indicates that the number of Brønsted acid sites of HMOR-parent, HMOR-A2, and HMOR-A1 is similar.

The FTIR spectrum showed a band at 3610 cm^{-1} (Fig. 9), which is associated with Brønsted acid sites, that means with hydroxyls bonded to framework aluminum (Si–OH–Al) [43,44]. The absorption band at 3740 cm^{-1} represents isolated silanol groups [45]. The FTIR spectra confirmed that the surface acidity of the leached mordenites was preserved. The decrease of the 3610 cm^{-1} peak is consistent with the decrease in the amount of Brønsted acid sites of HMOR-acid. This decrease is due to an increase in the framework Si/Al molar ratio after the acid leaching, leading to less aluminum in the framework. The number of terminal silanol

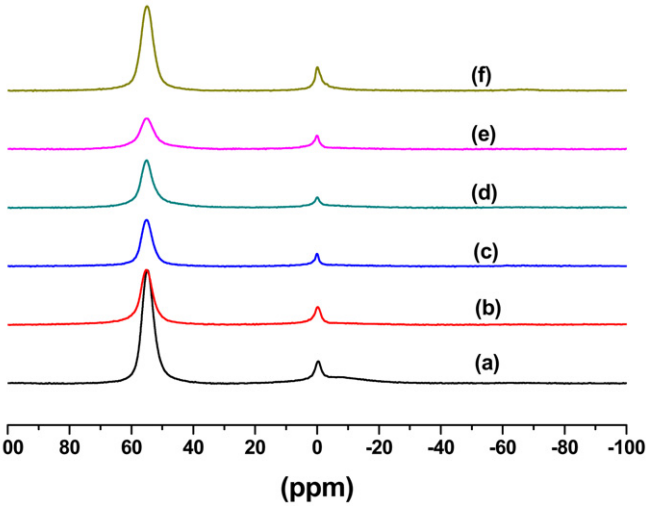

Fig. 8. ^{27}Al MAS NMR spectra of (a) HMOR-parent, (b) HMOR-acid, (c) HMOR-A1, (d) HMOR-A2, (e) HMOR-TPHAC, (f) HMOR-carbon.

groups (band at 3740 cm^{-1}) increased with increasing Si/Al molar ratio, because silanol groups are formed by dealumination [46]. The number of silanol groups increased when silicon atoms were extracted from the mordenite framework during the base leaching. These IR results confirmed that the order of the number of Brønsted acid sites in the three samples is HMOR-parent > HMOR-A1 > HMOR-acid and explained why the number of Brønsted acid sites of HMOR-parent and HMOR-A1 is similar.

3.2. Isomerization

The isomerization of 2M2P is a particularly useful reaction to probe the relative reactivity of solids of moderate acid strength be-

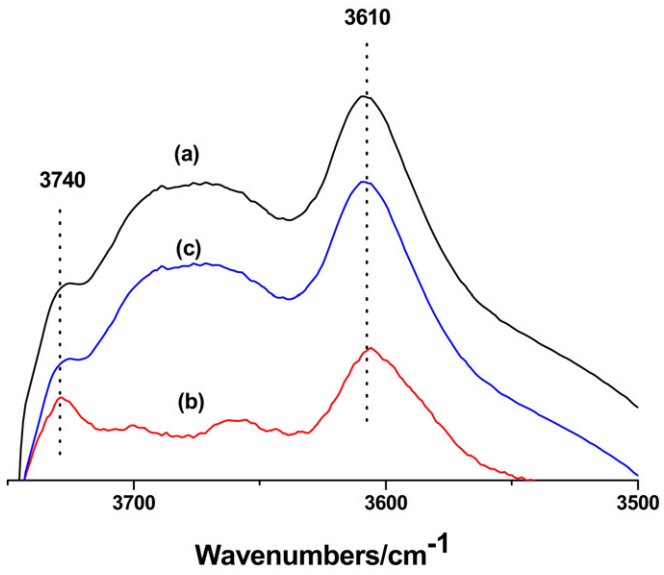

Fig. 9. FTIR spectra in the OH stretching region at 373 K: (a) HMOR-parent, (b) HMOR-acid, (c) HMOR-A1.

Table 3
Acidity evaluation of various mordenite samples.

Samples	Conversion (%)	Selectivity[a]	Selectivity[b]
HMOR-parent	32.0	0.19	0.30
HMOR-acid	23.4	0.27	0.58
HMOR-A1	54.9	1.23	1.12
HMOR-A2	52.8	1.11	1.05
HMOR-TPHAC	26.9	0.11	0.20
HMOR-carbon	23.2	0.14	0.30

[a] 3M2P/4M2P ratio at the conversion given in the second column.
[b] 3M2P/4M2P ratio at 50% conversion.

cause the alkene can convert to a large number of products whose relative rates of formation are expected to reflect the relative free energies of cationic intermediates [47,48]. The molar ratio of trans-3-methyl-2-pentene (trans-3M2P), obtained by methyl shift from 2M2P, to trans- and cis-4-methyl-2-pentene (trans- and cis-4M2P), obtained by hydrogen shift from 2M2P, reflects the reactivity of solid acids. The stronger the acid, the more readily will methyl group migration occur and the ratio of rates for the alkyl migration to double-bond formation is expected to increase. Namely, the higher the molar ratio is, the better a catalyst performs a more demanding reaction.

The conversion of 2M2P and the selectivity ratio (3M2P/4M2P) are shown in Table 3. The order of conversion of 2M2P over the different mordenites is HMOR-A1 > HMOR-A2 > HMOR-parent > HMOR-acid. At a conversion of 50%, the order of the selectivity ratio over the different mordenites is HMOR-A1 > HMOR-A2 > HMOR-acid > HMOR-parent. The selectivity ratio serves as a useful indicator of the reactivity of silica–alumina systems [48]. So we know that the order of reactivity of the different mordenites is HMOR-A1 > HMOR-A2 > HMOR-acid > HMOR-parent. However, the conversion of 2M2P over HMOR-parent was higher than that of the HMOR-acid, which can be explained by the different number of Brønsted acid sites on HMOR-parent and HMOR-acid. The number of Brønsted acid sites on HMOR-parent is much larger than that of HMOR-acid, therefore the conversion of 2M2P over HMOR-parent is higher than that of HMOR-acid. On the other hand, the number of Brønsted acid sites of HMOR-parent and HMOR-A1 is similar, but the conversion of 2M2P is higher than that of HMOR-parent, which can be attributed to the higher reactivity of HMOR-A1. For the same reason the conversion of 2M2P is higher on HMOR-A1 than on HMOR-A2.

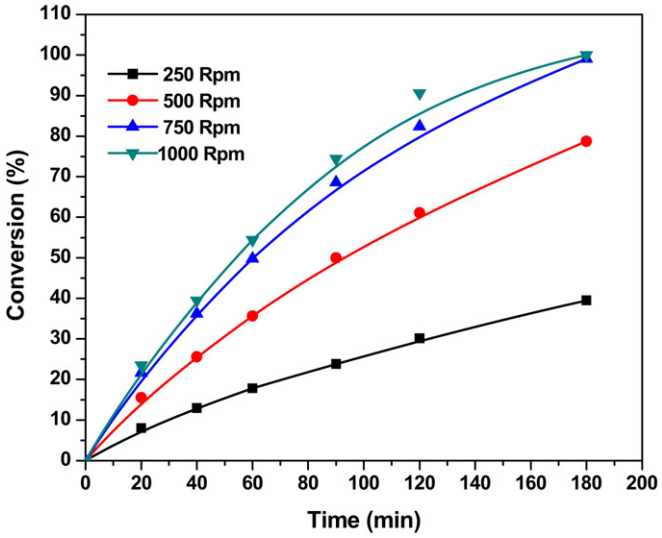

Fig. 10. Effect of speed of agitation on the alkylation conversion.

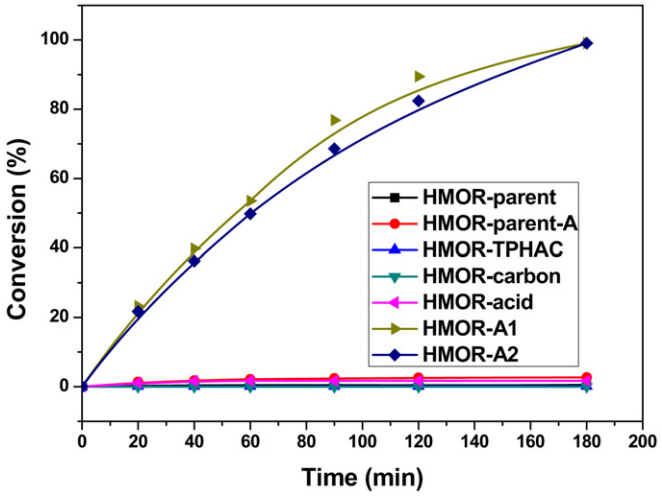

Fig. 11. Catalytic conversion of benzyl alcohol over different mordenite samples at 353 K.

3.3. Alkylation

Mesoporous zeolites may be the ideal catalysts for the Friedel–Crafts reaction of large molecules, because they overcome the diffusion limitation of zeolites on the reaction rate and also maintain the stability and strong acidity of conventional zeolites [49–51]. Thus, to confirm the presence of mesopores, the alkylation reaction of benzene with benzyl alcohol was measured.

To assess the role of external mass transfer on the reaction rate, the speed of agitation was varied between 250 and 1000 rpm using HMOR-A2 as catalyst (Fig. 10), keeping all other parameters constant. There was no big change when the speed was higher than 750 rpm, therefore all further runs were carried out at 750 rpm.

The conversion of benzyl alcohol in the benzylation of benzene over the different mordenites is shown in Fig. 11. The conversion of benzyl alcohol over HMOR-A1 and HMOR-A2 was near 100% after 3 h, but the conversion of benzyl alcohol on HMOR-parent, HMOR-parent-A, HMOR-acid, HMOR-TPHAC, and HMOR-carbon was less

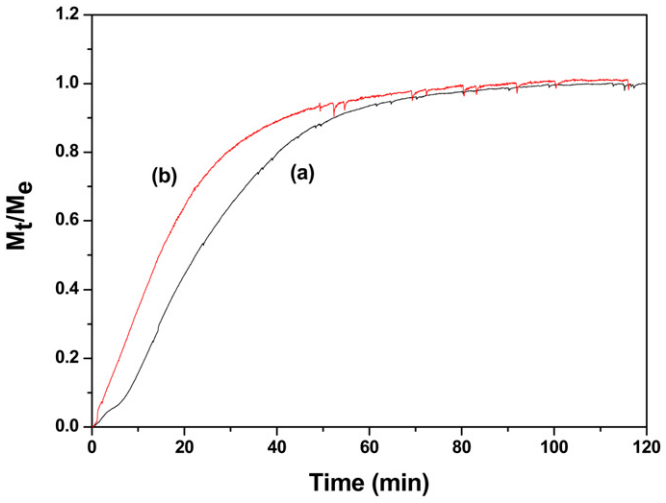

Fig. 12. The diffusion of toluene in (a) HMOR-parent, (b) HMOR-A1.

than 3%. The alkylation results are different from those of the isomerization, because the alkylation is decided by both the pore structure and acidity, while the isomerization is only decided by the number of acid sites and their reactivity. The formed diphenylmethane has a large size and mordenite does not provide enough space for this molecule to diffuse through the micropores. Mesopores enable diphenylmethane to escape from the mordenite crystal. Therefore, the conversion on the samples HMOR-parent, HMOR-parent-A, HMOR-acid, HMOR-TPHAC, and HMOR-carbon was very low, although some mesopores were found in HMOR-parent-A, HMOR-TPHAC, and HMOR-carbon. However, the mesopore volume is not enough or this mesoporosity comes from amorphous material without acidity. A rapid deactivation of these samples may be another explanation why they have a low conversion of alkylation of benzene with benzyl alcohol. Mesoporous HMOR-A1 had a higher conversion than HMOR-A2 because it has a higher mesopore volume than HMOR-A2 (Table 1). These results confirm that the alkylation reaction mainly occurs in the mesoporous parts of the mordenite.

3.4. Diffusivity

Since the molecular size of toluene is close to the pore size of mordenite zeolite, the diffusivity of toluene was determined to investigate the effect of the formation of mesopores on the improvement of the mass transfer ability in the mordenite framework.

For an isothermal system, the solution for the transient diffusion equation for a spherical particle is [52]

$$\Delta m_t = \Delta m_\infty \left[1 - 6/\pi^2 \sum_{j=1}^{\infty} \exp(-j^2\pi^2 Dt/R^2)/j^2 \right] \quad (1)$$

where Δm_t is the mass increase at time t, R_{eff} is effective diffusion length within the particle, and D is the diffusivity. The presence of mesopores in the particles with radius R will cause a shorter diffusion path length. When the adsorption and desorption reach equilibrium, the solution reduces to the approximate form [53]

$$\Delta m_t = \Delta m_\infty \left[1 - 6/\pi^2 \exp(-\pi^2 Dt/R^2) \right]. \quad (2)$$

Therefore, there is a linear relationship between $\ln(1 - \Delta m_t/\Delta m_\infty)$ and t and the slope of this straight line yields directly the intra-crystalline diffusion coefficient D.

The relation between M_t/M_e and diffusion time is shown in Fig. 12, where M_t and M_e denote the amounts of toluene adsorbed at time t and at adsorption equilibrium, respectively. Fig. 12 shows that the rate of adsorption of toluene into HMOR-A1 was larger than into HMOR-parent.

The SEM results showed that R of HMOR-parent was about 3.0 μm and R of HMOR-A1 was about 2.8 μm. The value (D/R_{eff}^2) of toluene in mesoporous HMOR-A1 was 2.6×10^{-3} s^{-1}, compared to 0.5×10^{-3} s^{-1} in HMOR-parent, which is about five-fold lower. This confirms that the mesopores in the mordenite framework increase the flux of toluene into the mordenite, by increasing the external surface area. The low diffusivity through HMOR-parent may also explain why the conversion of alkylation of benzene with benzyl alcohol is so low.

4. Conclusion

Three methods were investigated to synthesize mesoporous mordenite. The results show that without acid leaching (and diminishing of the aluminum content of the mordenite), base leaching of mordenite did not give as many mesopores as the method of acid leaching followed by base leaching. After acid leaching, however, the base leaching led to mesoporous mordenite that behaved very well in the isomerization and alkylation reactions. On the other hand, the synthesis with amphiphilic organosilane and carbon as secondary template did not lead to mesoporous mordenite.

The XRD, N_2 physisorption, SEM, and TEM showed that the leached mordenite is a crystalline mesoporous material with MOR framework. Acid leaching followed by base leaching appears to give mordenite with the best combination of microporosity, high surface area and external area, high mesopore volume, and strong acidity, leading to enhanced diffusion and accessibility of the micropores.

After acid and base leaching, HMOR-A1 and HMOR-2 showed a good activity in the isomerization of 2M2P, which can be attributed to their higher reactivity and larger number of Brønsted acid sites. Acid and base leaching enhanced the performance in the benzylation of benzene by benzyl alcohol. These results indicate that mesoporous mordenite obtained by acid leaching followed by base leaching has potential application in Friedel–Crafts alkylations, especially of large molecules. These good results may depend on the specific mordenite under investigation, because another synthesis procedure or mordenite may lead to different results in the acid leaching [54,55].

Acknowledgments

J.A. van Bokhoven thanks the Swiss National Science Foundation for financial support. Xianfeng Li thanks the China Scholarship Council (CSC) for financial support, and thanks Prof. Baojian Shen. We thank Yinyong Sun and Nadiya Danilina for helpful discussions and characterizations of samples.

References

[1] W.M. Meier, Z. Kristallogr. 439 (1961) 115.
[2] M. Tromp, J.A. van Bokhoven, M.T. Garriga Oostenbrink, J.H. Bitter, K.P. de Jong, D.C. Koningsberger, J. Catal. 190 (2000) 209.
[3] J.S. Jung, J.W. Park, G. Seo, Appl. Catal. A 288 (2005) 149.
[4] Y. Tao, H. Kanoh, L. Abrams, K. Kaneko, Chem. Rev. 106 (2006) 896.
[5] Y.N. Li, S.L. Liu, Z.K. Zhang, S.J. Xie, X.X. Zhu, L.Y. Xu, Appl. Catal. A 338 (2008) 100.
[6] C. Madsen, C.J.H. Jacobsen, J. Chem. Soc. Chem. Commun. (1999) 673.
[7] C.J.H. Jacobsen, C. Madsen, T.V.W. Janssens, H.J. Jakobsen, J. Skibsted, Microporous Mesoporous Mater. 39 (2000) 393.
[8] L. Tosheva, V.P. Valtchev, Chem. Mater. 17 (2005) 2494.
[9] R.A. Beidin, C. Choi-Feng, J.B. Hall, B.J. Huggins, G.J. Ray, Top. Catal. 4 (1997) 27.
[10] S. Bernasconi, J.A. van Bokhoven, F. Krumeich, G.D. Pirngruber, R. Prins, Microporous Mesoporous Mater. 66 (2003) 21.
[11] M. Boveri, C. Márquez-Álvarez, M.Á. Laborde, E. Sastre, Catal. Today 114 (2006) 217.

[12] K.-H. Lee, B.-H. Ha, Microporous Mesoporous Mater. 23 (1998) 211.
[13] R. Giudici, H.W. Kouwenhoven, R. Prins, Appl. Catal. A 203 (2000) 101.
[14] K.H. Chung, Microporous Mesoporous Mater. 111 (2008) 544.
[15] J.C. Groen, L.A.A. Peffer, J.A. Moulijn, J. Pérez-Ramírez, Microporous Mesoporous Mater. 69 (2004) 29.
[16] X.T. Wei, P.G. Smirniotis, Microporous Mesoporous Mater. 97 (2006) 97.
[17] J.C. Groen, T. Sano, J.A. Moulijn, J. Pérez-Ramírez, J. Catal. 251 (2007) 21.
[18] R. Srivastava, M. Choi, R. Ryoo, Chem. Commun. (2006) 4489.
[19] C.J.H. Jacobsen, C. Madsen, J. Houzvicka, I. Schmidt, A. Carlsson, J. Am. Chem. Soc. 122 (2000) 7116.
[20] Y. Tao, H. Kanoh, K. Kaneko, J. Am. Chem. Soc. 125 (2003) 6044.
[21] Z. Yang, Y. Xia, R. Mokaya, Adv. Mater. 43 (2004) 5880.
[22] B. Coq, V. Gourves, F. Figueras, Appl. Catal. A 100 (1993) 69.
[23] N. He, S. Bao, Q. Xu, Appl. Catal. A 169 (1998) 29.
[24] N. Narender, K.V.V.K. Mohan, S.J. Kulkarni, I.A.K. Reddy, Catal. Commun. 7 (2006) 583.
[25] Y.Y. Sun, R. Prins, Appl. Catal. A 336 (2008) 11.
[26] B.O. Hincapie, L.J. Garces, Q.H. Zhang, A. Sacco, S.L. Suib, Microporous Mesoporous Mater. 67 (2004) 19.
[27] K.J. Huttinger, M.F. Jung, Chem. Ing. Tech. 61 (1989) 258.
[28] X. Wei, P.G. Smirniotis, Microporous Mesoporous Mater. 89 (2006) 170.
[29] M. Ogura, S. Shinomiya, J. Tateno, Y. Nara, M. Nomura, E. Kikuchi, M. Matsukata, Appl. Catal. 219 (2001) 33.
[30] S.J. Gregg, K.S.W. Sing, Adsorption, Surface Area and Porosity, 2nd ed., Academic Press, London, 1982.
[31] J.C. Groen, J.C. Jansen, J.A. Moulijn, J. Pérez-Ramírez, J. Phys. Chem. B 108 (2004) 13062.
[32] J.C. Groen, J.A. Moulijn, J. Pérez-Ramírez, J. Mater. Chem. 16 (2006) 2121.
[33] G.J. Kim, W.S. Ahn, Zeolites 11 (1991) 745.
[34] G. Engelhardt, D. Michel, High-Resolution Solid-State NMR of Silicates and Zeolites, Wiley, New York, 1987.
[35] H. Stach, J. Jänchen, H.G. Jerschkewitz, U. Lohse, B. Parlitz, B. Zibrowius, J. Phys. Chem. 96 (1992) 8473.
[36] B.H. Wouters, T.H. Chen, P.J. Grobet, J. Am. Chem. Soc. 120 (1998) 1419.
[37] A. Omegna, J.A. van Bokhoven, R. Prins, J. Phys. Chem. B 107 (2003) 8854.
[38] A. Abraham, S.H. Lee, C.H. Shin, S.B. Hong, R. Prins, J.A. van Bokhoven, Phys. Chem. Chem. Phys. 6 (2004) 3031.
[39] J. Jiao, J. Kanellopoulos, W. Wang, S.S. Ray, H. Foerster, D. Freude, M. Hunger, Phys. Chem. Chem. Phys. 7 (2005) 3221.
[40] P.E. Eberly, C.N. Kimberlin, A. Voorhies, J. Catal. 22 (1971) 419.
[41] D.K. Thakur, S.W. Weller, J. Catal. 24 (1972) 543.
[42] D.K. Thakur, S.W. Weller, Adv. Chem. Ser. 121 (1976) 596.
[43] A. Corma, M. Grande, V. Fornes, Appl. Catal. 66 (1990) 45.
[44] A. Zecchina, S. Bordiga, G. Spoto, D. Scarano, G. Petrini, G. Leofanti, M.J. Padovan, J. Chem. Soc. Faraday Trans. 88 (1992) 2959.
[45] A. Zecchina, S. Bordiga, G. Spoto, D. Scarano, G. Petrini, G. Leofanti, M.J. Padovan, Phys. Chem. 96 (1992) 4991.
[46] B.H. Ha, D. Barthomeuf, J. Chem. Soc. Faraday Trans. I 75 (1979) 2366.
[47] G.M. Kramer, G.B. McVicker, J.J. Ziemiak, J. Catal. 92 (1985) 355.
[48] G.M. Kramer, G.B. McVicker, Acc. Chem. Res. 19 (1986) 78.
[49] Y. Tal, H. Kanoh, K. Kaneko, J. Am. Chem. Soc. 125 (2003) 6044.
[50] S. Kim, J. Shah, T. Pinnavaia, Chem. Mater. 15 (2003) 1664.
[51] M. Hartmann, Angew. Chem. Int. Ed. 43 (2004) 5880.
[52] J. Crank, in: The Mathematics of Diffusion, Oxford Press, London, 1975.
[53] J. Karger, D.M. Ruthven, in: Diffusion in Zeolites and Other Microporous Solids, Wiley, New York, 1992.
[54] J. Garces, J.J. Maj, G.J. Lee, S.C. Rocke, US Patent 4,891,448 (1990).
[55] P.R. Rudolf, J.M. Garcés, Zeolites 14 (1994) 137.